Computer simulations of radiation damage in amorphous solids

J. Laakkonen* and R. M. Nieminen
Laboratory of Physics, Helsinki University of Technology, Otakaari 1, SF-02150 Espoo, Finland
(Received 24 March 1989)

Microscopic radiation damage in a Lennard-Jones amorphous solid is investigated by computer simulations of collision cascades. Molecular-dynamics simulations with various primary knock-on atom (PKA) energies and directions are carried out. Energy outflow from the computational box is accounted for but electronic losses are neglected. The simulations show the PKA energy to spread rapidly among the nearby atoms, and the atomic trajectories disclose such features as replacement collision sequences and focused chains. Vacancies are created in the central region of the cascade and are surrounded by a cloud of interstitials. The defects mainly disappear independently of each other, the vacancies faster than the interstitials. Recombination plays a minor role. At the end of a simulation all the defects created have vanished and little change in the sample volume or structure is observed. The threshold energy for a permanent displacement is found for various PKA directions. The validity of the modified Kinchin-Pease model for an amorphous solid is discussed.

I. INTRODUCTION

When a fast moving particle traverses a solid, it strikes the host atoms, transferring large amounts of kinetic energy. The energy received by the primary knock-on atoms (PKA's) usually far exceeds the bond energy, and thus a PKA initiates a sequence of successive collisions, a collision cascade. The outcome of a collision cascade is a large amount of point defects, i.e., vacancies and interstitials. A vast majority of the defects vanish during or soon after the cascade is over, but some may survive, increasing the defect content of the solid over the thermodynamic-equilibrium concentration. Under suitable circumstances point defects can subsequently agglomerate, creating larger defect formations, and thus a complex defect structure may follow, giving rise to changes in many physical properties.

Formation of a collision cascade is a complex many-particle event and no comprehensive, analytic framework including, for instance, the effects of the structure of the solid or the forces between the atoms does exist. The few attempts made treat the cascade, e.g., as a suddenly heated region (a thermal spike) or a volume, where a miniature "explosion" has taken place at the position of the PKA (a displacement spike). The advance of the cascade is then followed by assuming the solid to be a homogeneous medium and by applying the classical laws of heat conduction or shock waves. Obviously, these kind of models cannot disclose the real structure or the many details of the cascade. If not the form of the cascade itself but its outcome (the number of defects) instead is considered, then the statistical models first introduced by Kinchin and Pease[1] have been applied to some extent. One computational method capable of yielding a wealth of information about the collision cascade is direct computer simulation. The applicability of this method is now rapidly improving along with the progress in computer capacity and the advances made in the fields of simulation algorithms and potential functions for interactions between particles.

For collision cascades there are two possible simulation methods: in the case of low and moderate PKA energies the full molecular-dynamics (MD) simulation is preferable, whereas for high PKA energies [$E_{\mathrm{PKA}} > (100-1000)E_d$, where E_d is the displacement energy] the binary-collision approximation (BCA) is appropriate. In the MD simulations one considers all the particles, while in the BCA method a lower limit is set for the kinetic energy of the atoms that are followed. Both methods have been widely applied.[2] The preceding methods (especially MD) compute the actual trajectories of the particles, and they are used to simulate the collisional and the cooling phases of the cascade during which most of the defects produced have already disappeared. This corresponds to real time of approximately 10^{-11} s. During later stages the defects left will diffuse causing recombination and clustering, or they may become trapped into sinks such as dislocations and grain boundaries. These effects take much longer times, rendering the MD simulation impractical since it would require vast amounts of computer time. The solution is to apply for the diffusion of defects of a Monte Carlo–type simulation.[2–4]

The foundations of MD simulations of collision cascades were laid by the classic work of Gibson *et al.*, who studied radiation damage in crystalline copper.[5] Since then basically the same methods have been repeatedly applied. Along with experimental data, these studies have contributed much to our understanding of the formation radiation damage in crystalline materials. This makes it surprising that radiation damage in the other type of solids, amorphous materials, has hardly been studied at all. These materials have many properties distinctly different from those typical for crystalline structures. Often these exceptional characteristics are also of technological importance. The few studies of radiation damage in amorphous metals show that metal-metalloid glasses have a good resistance against radiation effects.[6,7] Then,

combined with their high mechanical strength, such materials would be most useful as construction materials in nuclear technology.

In this work the MD simulation is used to study radiation damage in a prototype amorphous solid. The sample is a one-component system, where the interactions between the atoms are described by the Lennard-Jones potential. This potential best approximates the noble-gas atoms, whereas real metallic glasses are alloys of two or more constituents and the potentials are not necessarily of the two-particle type. However, we expect to expose some of the characteristics generic to radiation damage in amorphous solids. Although the absolute energy scales of noble gas and metallic systems are very different, collision cascades corresponding to impact energies scaled by the displacement thresholds enable qualitative comparison between different materials. In many respects the one-component Lennard-Jones system is also a much studied reference case.[8] It is thus of interest to know its irradiation behavior. In this report we present the results of 30 collision-cascade simulations done for a sample of 1372 atoms. The PKA energies studied range from about $1E_d$ to $80E_d$. Ten different PKA's and directions are used. In Sec. II we describe the simulation method and consider the definition and identification of point defects in amorphous materials. Before starting with the radiation damage simulations we first determine in Sec. III the value of E_d for the amorphous Lennard-Jones system. Section IV deals with the energy outflow through the computational box surfaces during a cascade simulation. The collision-cascade simulations are presented in Sec. V with analyses of the cascade structure, point defects, and other related data. The results are discussed in Sec. VI, and Sec. VII contains a summary of the main findings.

II. METHOD

The sample for computer simulations here is the same as studied before in two earlier papers (Refs. 9 and 10, referred to hereafter as I and II, respectively). This is a one-component amorphous noble-gas solid of 1372 atoms. The potential experienced by an atom is obtained as a sum of pairwise interactions of the Lennard-Jones form:

$$\phi(r)=4\varepsilon\left[\left[\frac{\sigma}{r}\right]^{12}-\left[\frac{\sigma}{r}\right]^{6}\right]. \tag{1}$$

This same functional form applies to all noble gases, and thus the results describe all noble gases for appropriate values of ε and σ. To exploit this scaling, here we use reduced units (abbreviated in text as r.u.): the units of length and energy are σ and ε, respectively, the unit for temperature is ε/k_B and the unit for time $(M\sigma^2/\varepsilon)^{1/2}$, M being the atomic mass. As a specific example here we consider neon, for which[11] $\varepsilon/k_B=35.3$ K, $\sigma=2.8509$ Å, and $M=3.351\times10^{-26}$ kg. With these values the time unit is 2.364×10^{-12} s.

In MD simulation one numerically integrates the classical Newtonian equations of motion. Here the algorithm by Beeman[12] is used. To compute the forces the potential (1) is truncated at $r=2.61$ r.u. (=7.45 Å for Ne), which for a crystalline fcc lattice is the distance up to between the fifth- and sixth-nearest neighbors. The integration time step Δt varies depending on the stage of the collision cascade: it is changed continuously during the cascade according to the criterion that during one time step the fastest atom moves at the most 0.035 r.u. (0.1 Å for Ne). At the end of a cascade simulation, when the system is near equilibrium at a low temperature and the atoms can be considered as vibrating around their equilibrium positions, the time step is set by the requirement that one atomic vibration should last (20–30) Δt. Accordingly, the maximum value of Δt used in the simulation is 0.0296 r.u. ($=7\times10^{-14}$ s for Ne). The use of periodic boundary conditions is a standard procedure in MD simulation to extend the computational cell into a pseudoinfinite arrangement, removing thereby the effect of the boundaries. This is used here also except for the initial stage of a cascade, when a large amount of energy is injected in the computational cell and the energy flow out of the cell must be accomplished in some way. We shall return to this question later. The temperature and the pressure at a given time are determined in the usual way from the average kinetic energy per particle and the virial theorem, respectively.

The amorphous sample was prepared by a computer-simulated rapid quench from a liquid state (for details see I). The pair distribution function of the amorphous structure obtained is in very good agreement with other studies, as discussed in I and II. The sample temperature has been lowered in this study to 0.001 48 r.u. (0.0522 K for Ne) from the previous 0.122 r.u. used in I and II. The external pressure is zero. The identification of vacancies and interstitials is an integral part of the analyses of any radiation damage study. For amorphous solids, however, this is not straightforward and therefore a detailed study was made in II to create working methods to be used in extracting point defect information from MD data. For consistency we briefly repeat here the procedure given in II for characterization of point defects in an amorphous Lennard-Jones solid.

To find vacancies a cavity analysis is used: At first a sphere of radius r is attached with each atom:

$$r=(4\sqrt{2}n)^{-1/3}, \tag{2}$$

where n is the mean atomic density. Then the space between the atomic spheres is filled with nonoverlapping, empty spheres (cavities) as large as possible. Nearby cavity spheres will form a cluster, if (i) all the cavity spheres in the cluster have a volume larger than 0.076 r.u. (ii) at least one of the spheres of the cluster has a volume larger than 0.129 r.u., and (iii) the surface of each cavity sphere is closer than 0.274 r.u. to some other cavity sphere belonging to the same cluster. Given this, a monovacancy is identified as a single cavity with volume larger than 0.26 r.u. or as a cavity cluster with volume in the range 0.32–0.49 r.u. The volume V_c of a cavity cluster for a divacancy varies between $0.49\le V_c\le0.74$, for a 3^- vacancy between $0.74\le V_c\le0.98$ and for a 4^- vacancy $V_c\ge0.98$ r.u.

The interstitials are found by computing the local hydrostatic press p_i at each atom from

$$p_i = \frac{1}{6\Omega_i} \sum_{j(\neq i)} \frac{\partial \phi}{\partial r}\bigg|_{r_{ij}} r_{ij} \ , \tag{3}$$

where r_{ij} is the distance between atoms i and j. The atomic volume Ω_i is computed as

$$\Omega_i = \frac{4\pi}{3} a_i^3 \ , \tag{4}$$

where

$$a_i = \frac{\sum_j r_{ij}^{-1}}{2\sum_j r_{ij}^{-2}} \ . \tag{5}$$

The summation in (5) extends just beyond the nearest neighbors. The interstitials have large negative pressure and in II a limiting value for the interstitial pressure p_0 was proposed. This depends on the external pressure $\bar{p}$ as

$$p_0 = 1.736\bar{p} - 12.230 \ . \tag{6}$$

To exclude the borderline cases, here we increase the value given earlier by 10% and identify interstitials as those atoms having a pressure $p_i < 1.1p_0$. The temperature dependence of p_0 was found to be weak up to half the glass transition temperature. Beyond this $|p_0|$ starts to increase roughly linearly with temperature. In a collision cascade the temperature first increases sharply, but the increase, however, is transient and applies only to the cascade atoms. Under these conditions the use of an unequivocal temperature is doubtful, and as a result the temperature dependence of p_0 is not considered here.

III. DISPLACEMENT THRESHOLD ENERGY

The threshold energy for producing permanently displaced atoms (displacement threshold in short) E_d is defined as the kinetic energy an atom must have to leave its equilibrium site and not to return. For a crystal this means formation of a vacancy-interstitial pair (a Frenkel pair) and the value of E_d is the minimum energy for such a defect to be stable against recombination. In the case of an amorphous structure the situation is different: when an atom is displaced, the empty space at the original atomic position can readily be filled by several small movements of the neighbor atoms or by one large leap of a single atom. Likewise the displaced atom can easily "dissolve" in the material at its new position and is not necessarily counted as an interstitial. For this reason it is obvious that as a result of an atomic displacement in an amorphous structure anything analogous to a Frenkel pair of a crystal does not necessarily form. Therefore we monitor E_d from the changes in the atomic positions instead of the appearance of a vacancy-interstitial pair.

The displacement threshold depends on the direction of the atomic movement. In amorphous systems there is no crystalline order to define directions and local concepts must be used instead. We do this by seeking three atoms in the middle of the computational box, all of which are nearest neighbors to each other. The distances between the atoms found (labeled as A, B, and C) are 1.03, 1.08, and 1.09 r.u., while the first maximum of the pair distribution function of the sample occurs at 1.07 r.u. We take the atom A as origin and divide the line BC into four equal parts. Then the vectors from A to B, C, and the three dividing points define five directions. Other directions are found by creating a plane, which is perpendicular to the plane formed by atoms A, B, and C and which includes the atom A and the center point of the line BC. The positions of the atoms at this plane and nearby are shown in Fig. 1. We scan this plane for the full circle in steps of 15°: the direction 0° is the atom A moving towards the center of line BC, and positive and negative angles are from this in the counterclockwise and clockwise directions, respectively.

The value of E_d for a given direction is found by giving the atom A (called the test atom) impulses of varying energy and looking for the threshold value, at which atomic displacements of the order of one nearest-neighbor distance emerge. Each run simulates 510 time steps (about 3.6 r.u. of real time) and the difference of the positions at the first and last time steps are computed for each atom. The distribution of the position differences is found to be

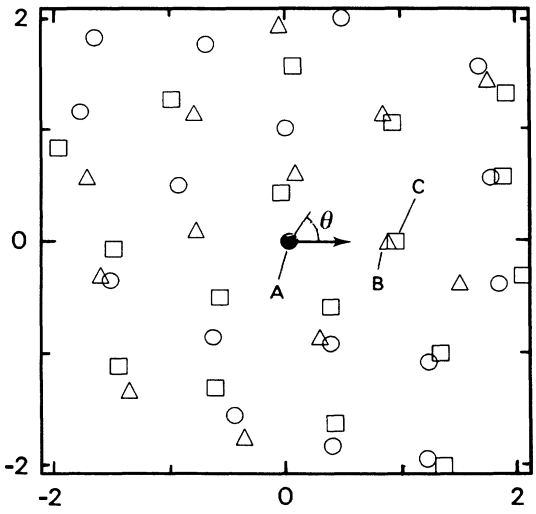

FIG. 1. Positions of atoms at the plane, where the displacement threshold energy is studied. The test atom (A) is shown as a solid circle and is situated in the middle of the volume plotted. Direction 0° is indicated by an arrow. Atoms in this and the following figures are plotted as follows: the volume plotted is a rectangular box that has two edges of equal lengths and that lie in the plane of the paper (x and y directions). The length of these varies from plot to plot and can be seen from the figure. The third edge (z direction) is always 2.806 r.u. long. The box is divided in the z direction into three equal smaller boxes. An atom is now shown as a triangle, circle, or a square depending whether it is in the uppermost, middle, or lowest box, respectively. The length 2.806/3 r.u. in the z direction makes each of the boxes to be slightly less than the nearest-neighbor distance and thus each of the boxes show only one "atomic layer." Reduced units (r.u.) are used in this and all the other figures.

continuous and reaching up to ~0.63 r.u. However, if the energy has been large enough distinct displacements of 0.8 r.u. and larger can be seen. Initially the sample has the temperature of 0.001 48 r.u. (0.0522 K for Ne) and the pressure is zero. Since only small energies are considered, we apply here the regular constant volume simulation with periodic boundary conditions.

Figure 2 shows the displacement of the test atom as a function of the kinetic energy given to it. The direction of the impulse is 16.7° from the 0° direction towards atom *B* (i.e., in the *ABC* plane perpendicular to the plane of Fig. 1). It is seen that initially the displacement is very small, but at 292 r.u. (0.8875 eV for Ne) it suddenly jumps up to 0.83 r.u. and changes only slightly when the energy is further increased. The test atom has clearly experienced a displacement from one equilibrium position to another. The atomic movements are shown in Fig. 3, where the test atom is seen to initiate an actual sequence of replacement collisions. A supplement run simulating an additional 3000 time steps confirms that the replacements of the test atom and the next three atoms along the chain are permanent. Figure 4 shows that the kinetic energy is transferred from atom to atom very efficiently along the chain and, for example, the test atom itself is seen to give off nearly all of its kinetic energy. Note that the maxima of kinetic energy for the other permanently displaced atoms are considerably less than what is needed for the test atom to get displaced. Figures 3 and 4 are examples of the property of a collision cascade to form chains that resemble focused collisions in crystalline structures and, correspondingly, in the following we use the concept of a focused collision also for amorphous systems. Figure 3 is seen to exhibit also a replacement collision sequence.

Figure 5 shows the energy dependence of the displacement for $\Theta = 45°$ in the plane of Fig. 1. As shown earlier in Fig. 2, the change in the displacement is very clear. Now this happens at a much lower energy of 133 r.u., yet the displacement (1.46 r.u.) is larger than before. It is interesting to see that the test atom displacement stays approximately constant up to rather high energies of 1200 r.u., when another jump to 2.5 r.u. occurs. The stepwise structure is obviously a result of the form of the

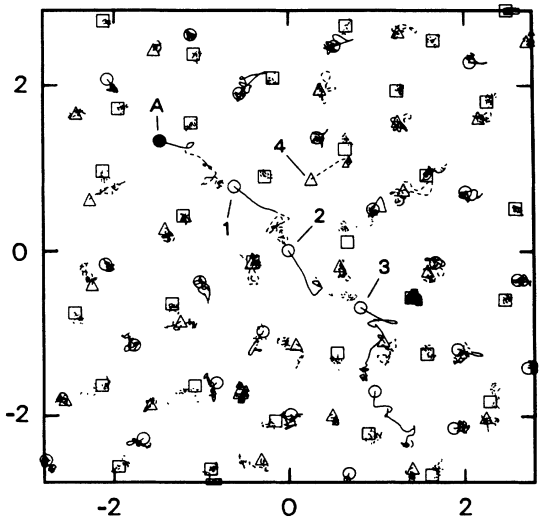

FIG. 3. Atom movements for the threshold energy (292 r.u.) of Fig. 2. In the plot 3.98 r.u. of real time is simulated. The large symbols show the initial positions of the atoms (cf. Fig. 1). Trajectory of an atom is shown by a line, the type of which indicates the box (*z* coordinate), where the atom is moving: dashed for the uppermost, solid for the middle, and a dotted line for the lowest box. A small symbol shows that an atom has left (or entered) the plotting volume; the symbol type has the same meaning as for initial positions.

potential-energy surface: an atom must be given enough energy to leap from one local minimum to another; if the energy is not enough the atom stays at its position and gives the excess energy to its neighbors. A study of the atomic movements reveals that in this case the test atom does not force any atom to leave its site, but the test atom finds itself a new site between the neighbor atoms. The former site of the test atom is filled by one atom, whose empty position is then taken over by another atom.

In the two preceding cases discussed, the test atom experiences a sharp increase in the displacement when the

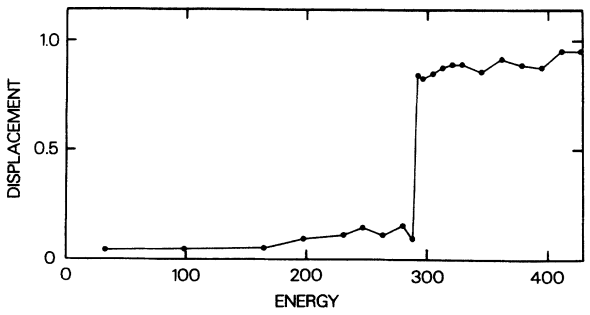

FIG. 2. Displacement of the test atom as a function of kinetic energy given to it. For the direction see the text. The lines connecting the symbols are drawn only to guide the eye.

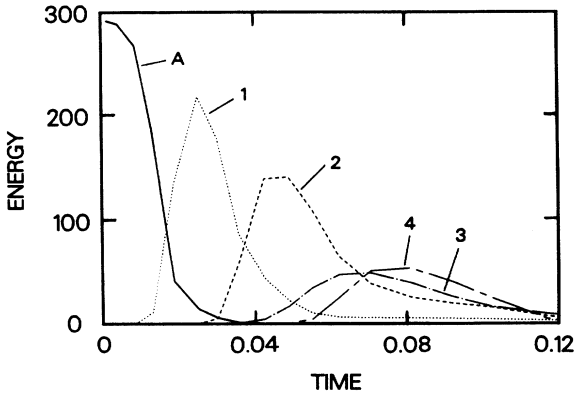

FIG. 4. Kinetic energy of the labeled atoms of Fig. 3 as a function of time. Other atoms of Fig. 3 receive much less energy than the labeled ones.

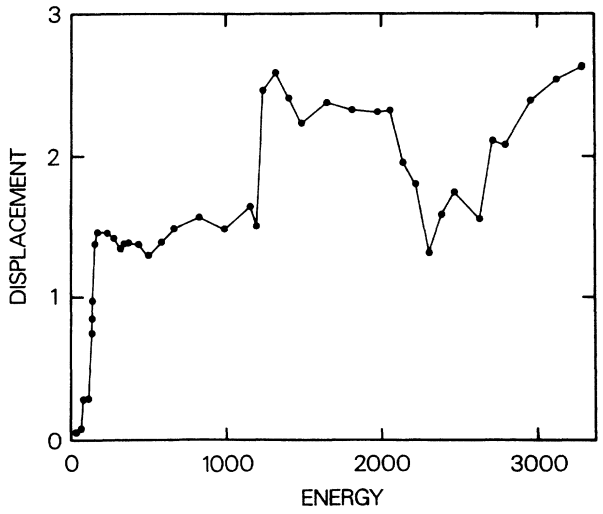

FIG. 5. Displacement of the test atom as a function of kinetic energy given to it. Direction of movement is 45° in the plane of Fig. 1.

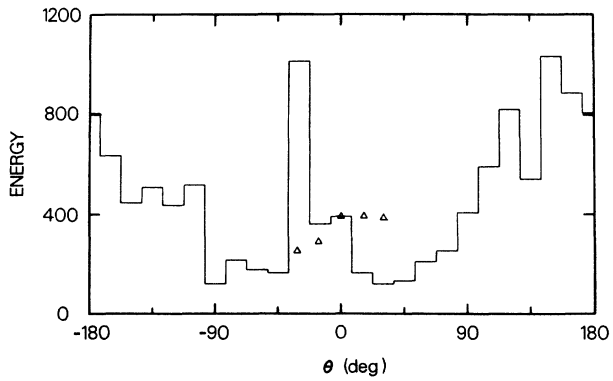

FIG. 6. Displacement threshold energy as a function of direction in the plane of Fig. 1. The triangles show threshold energy for directions at a plane perpendicular to the plane of Fig. 1; the rightmost and leftmost triangles are head-on directions towards the two adjacent nearest neighbors (atoms *B* and *C*) of the test atom.

kinetic energy exceeds a certain value. This, however, need not always be the case, and a few directions have been found where the displacement has no stepwise form. In these cases the energy of the test atom is distributed rather evenly by many atoms, and as a result it is difficult for any atom to make a distinct displacement. By increasing the energy large displacements finally emerge, but because of the complex energy distribution the displacement may fall down with increasing energy when new scattering channels become possible.

The preceding discussion shows that when the test atom is given an energy impulse large enough, then the atom, one or more of its neighbors, or both will get displaced by about one nearest-neighbor distance. We define the displacement threshold E_d in a given direction to be the lowest test atom energy, when any atom makes such a displacement. Figure 6 shows the results of the displacement threshold simulations for directions in the plane of Fig. 1. Also the five directions in the plane *ABC* are shown. The inaccuracy of the points is 5% or less. One immediately observes the large variation of E_d from 118 to 1040 r.u. The minima occur at 30° and −90°, the former of which corresponds to an "easy or open direction" (see Fig. 1) and the only displacement is due to the test atom itself. In the latter case the displacement is made by one of the neighbors, which moves into one of its easy directions after receiving energy from the test atom. The local maxima of E_d at −30°, 120°, and 150° are all cases, where many atoms receive a sizable portion of the test atom energy. Note that a direct hit towards a nearest-neighbor atom or just between a pair of them does not result in a maximum nor a minimum of E_d. The average displacement threshold energy computed from the figure is 440 r.u.

Using the definitions given in Sec. II for point defects, it is possible to study their existence during an atomic displacement in amorphous solids. For a vacancy we find that when an atom is being displaced, the former atomic site is initially identified as a vacancy but disappears soon (in about 0.8 r.u.) through the movements of nearby atoms. The displaced atoms themselves behave as interstitials, but only for a very short time (about 0.08 r.u.). After this time their new neighborhood has readjusted itself and the displaced atoms are no longer identified as interstitials. The stability of the atomic arrangements after a displacement has been tested by extending some of the regular 550 time step runs another 3000 time steps more. These show no novel features, and the displaced atoms are seen to stay at their new positions.

IV. ENERGY DISSIPATION AT BOUNDARIES

In a collision event the energy received by the PKA is first transferred into kinetic energy of the cascade atoms and the cascade volume heats up considerably. After this, heat is quickly transported away to other parts of the solid and the temperature of the cascade volume decreases. From the computer simulation point of view the solid away from the cascade body represents a heat sink and, unless the PKA energy is small or the sample large, this must be accounted for somehow. A natural way is to use boundary conditions that make possible energy to flow out of the computational box through the surfaces. Obviously the traditional periodic boundary conditions do not fulfill this, since they do not allow a particle as well as energy to leave the computational box.

One way to accomplish energy outflow at surfaces is to add a dissipative force component to the equations of motion for atoms near the surface. The dissipative force is proportional to the particle velocity and provides a means of energy consumption. The proportionality constant is chosen to minimize boundary reflection.[5,13] Beeler[2] even gives a formula based on an analogy of a damped, one-dimensional oscillator. In addition to the dissipation, other considerations are needed for the surface atoms. Gibson *et al.*[5] take the atoms outside the computational box into account by applying two other additional forces on the surface atoms: a constant force

and a spring force. The former accounts for the cohesion due to conduction electrons, and the latter is used to describe the material resistance for slow deformations of the solid. King and Benedek just keep the surface layer of atoms fixed.[13] Beeler suggests representing the atoms beyond the boundary region as an elastic continuum. A slight disadvantage is that each of the methods described calls for modifying the integration schemes for position and velocity of the surface atoms. Also the choice of the various force constants is not unequivocal. For these reasons we use another method, which requires minimal changes in the simulation algorithm and yet provides for the energy outflow in a reasonable way.

We start with the periodic boundary conditions but, in addition, define a boundary region at the surface so that the atoms inside the boundary region are treated in a special way: the kinetic energy of these atoms is computed periodically, and if this exceeds a given limit then, retaining the direction, the atomic velocity is scaled down to some low value. In this way the integration algorithms need not be changed, and no new forces are needed, since the boundary atoms feel the interaction of the atoms at opposite surfaces because of the repetition of the computational box through the periodic boundary conditions. We call this procedure an application of a heat bath. Parameters in this model are the thickness of the boundary region, a scaled down limit for kinetic energy, kinetic energy after scaling, and time between successive scalings. These are chosen so that (i) the energy outflow approximates an infinite sample, (ii) reflection at cell boundaries is at minimum, and (iii) the volume of the boundary region is as small as possible. The first two criteria above favor a thick boundary with few scalings, which is in conflict with the third requirement, and thus a compromise is needed.

The first parameter set studied has a thin boundary region, the thickness of which is only 0.35 r.u., this being less than the nearest-neighbor distance. Within the boundary region the velocity of atoms having kinetic energy above 0.0078 r.u. is scaled down to a Maxwellian velocity distribution with average kinetic energy of 0.0014 r.u. (this corresponds to temperature 0.05 K for Ne). The

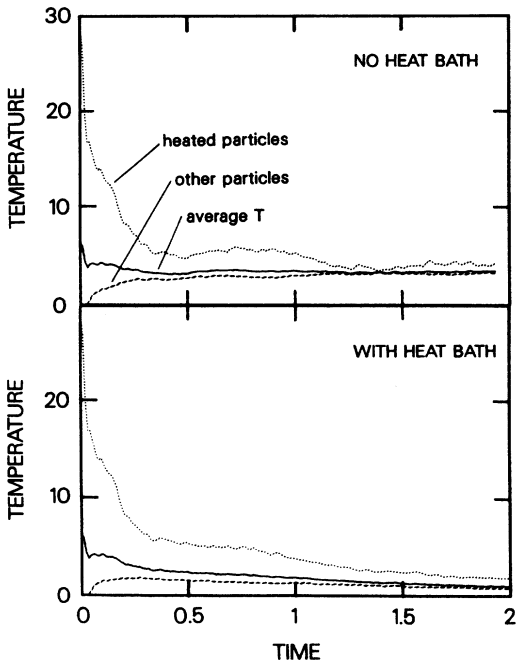

FIG. 7. Cooling of the 300 heated atoms in the cases of no heat bath and with heat bath. The average temperature and temperatures of the heated and not heated atoms are shown.

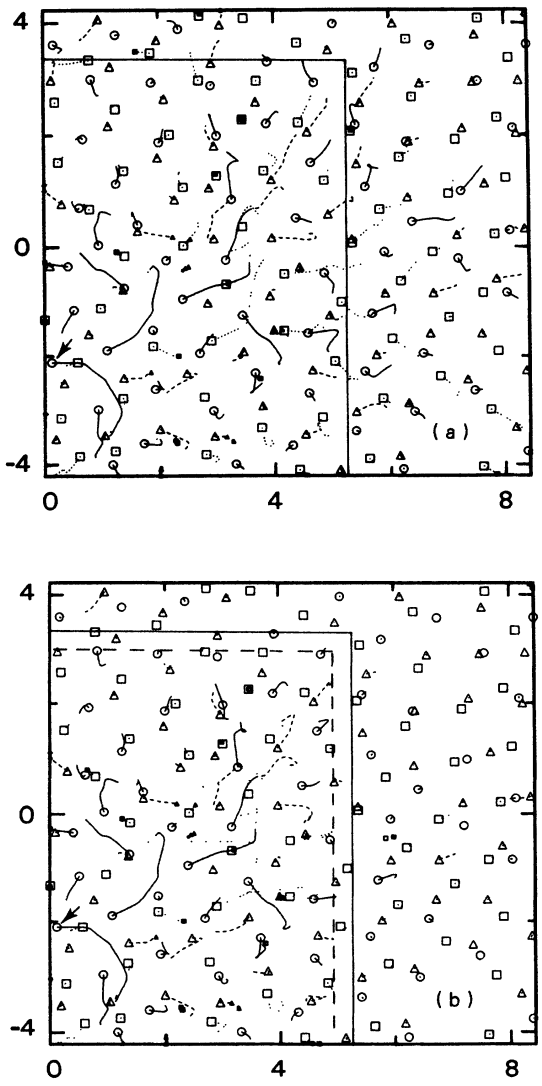

FIG. 8. Atomic trajectories showing the effect of the heat bath. The initial position of the PKA is indicated by an arrow and the energy given is 10 000 r.u. The plotted volume is oriented parallel with the computational cell. Solid lines mark the computational box surfaces, and the dashed line in (b) indicates the boundary of the heat bath region. In (a) no heat bath is used, and trajectories span time 0–0.191 r.u. (b) is obtained with a heat bath; the time interval is 0–0.208 r.u.

scaling is done every fifth time step. The energy outflow is tested by setting the kinetic energy of 300 atoms in the center of the computational box to 28.3 r.u. (1000 K for Ne), while the rest of the 1372 atoms are initially at temperature 0.0015 r.u., and by monitoring the cooling of the heated atoms. The 300 atoms are situated within a radius of 4.10 r.u. from the center of the computational box. The upper part of Fig. 7 shows the various temperatures as a function of time with regular periodic boundary conditions and no heat bath applied. An interesting feature is the bumps in the temperature of the heated atoms appearing first from 0.5 to 1.2 r.u. with the second one starting around 1.5 r.u. The bumps result from the periodic boundary conditions, which return the heat pulse back to the center. This, of course, is a spurious effect. A real effect, on the contrary, is that a part of the heat pulse can be reflected back from the cold atoms affecting the cooling of the hot atoms, but this would happen sooner and not until a time lag of 0.5 r.u.; in fact, some delay is seen in the temperature decrease of the hot atoms during a period from 0.07 to 0.2 time units. The dip in the average temperature at 0.035 r.u. marks the time when the initial excessive kinetic energy is partitioned in correct proportions into kinetic and potential energies. The effect of the heat bath is evident in the lower part of Fig. 7, which shows the results of a simulation like the preceding one but using a heat bath with the parameters given. The bumps in temperature have now vanished and the temperature decreases steadily. A slight reminiscence of a bump around 0.8 r.u. is probably due to some energy reflecting from the boundary region.

In addition to making energy outflow possible, the heat bath should not distort the cascade structure inside the computational box. To study this we have made two cascade simulations, giving a kinetic energy of 10 000 r.u. to an atom in the center of the box and recording the atomic trajectories with and without the heat bath. The atomic trajectories are shown in Fig. 8(a) for no heat bath and in Fig. 8(b) with heat bath used. The surface of the computational box is also plotted, and the dashed line in Fig.

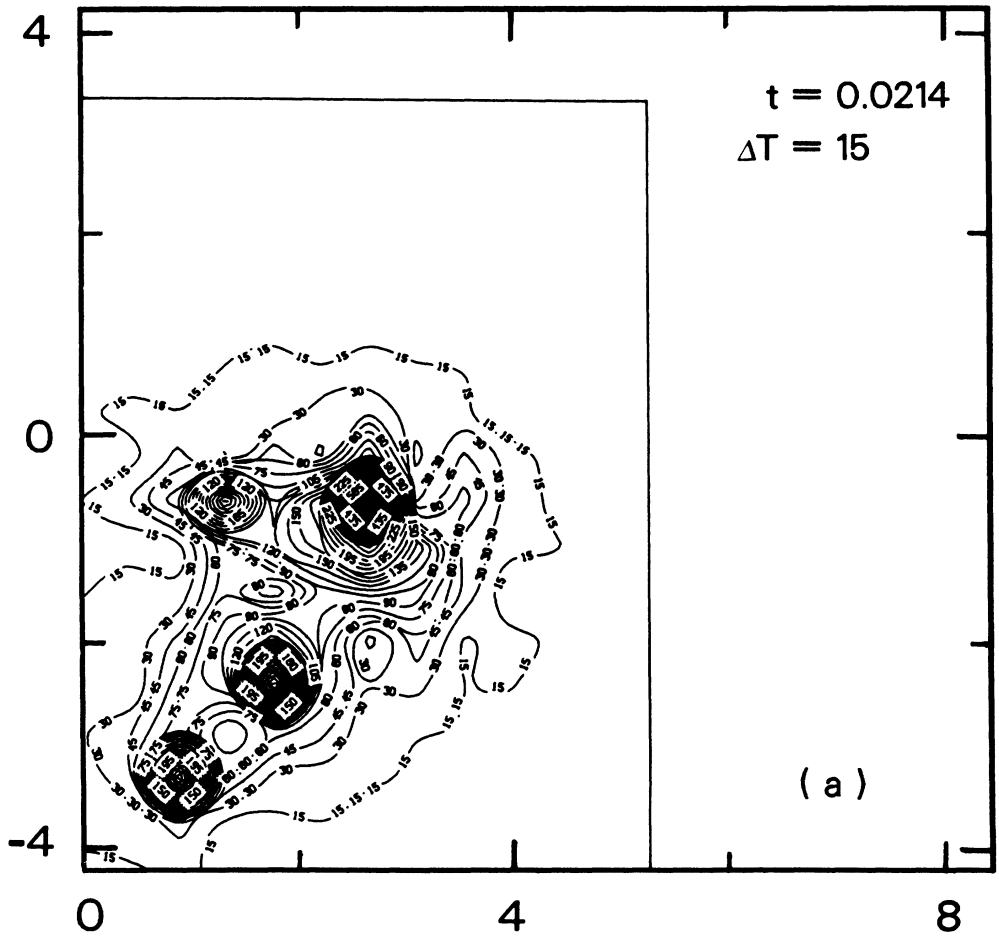

FIG. 9. Spreading of kinetic energy during the simulation of Fig. 8(a) (i.e., no heat bath is used). The contour lines show the constant kinetic energy values of the atoms inside the plotting volume, which is the same as in Fig. 8. The time instant (t) and the contour spacing (ΔT) are shown in each plot. Note that ΔT refers to the average kinetic energy per atom, which is now not the same as the temperature because of a component of net outward motion in the cascade.

8(b) shows the boundary of the heat bath region. From Fig. 8(a) one clearly sees how the cascade proceeds beyond the computational box, but because of the periodic boundary conditions it in fact enters the same box from the opposite side. When the heat bath is used [Fig. 8(b)], the cascade terminates very effectively at the box surface; only two small branches succeed in escaping through the heat bath region. The atomic trajectories in the heat bath region and in its immediate vicinity differ, of course, but for trajectories of the other atoms the effect of the heat bath is remarkably small. Figures 9 and 10 describe the spreading of kinetic energy for the cascades of Figs. 8(a) and 8(b), respectively. Each contour plot shows the constant kinetic energy distributions of the atoms inside the plotting volume at the time given. In Fig. 9(a) a few collisions have occurred, and the energetic atoms are shown as a number of concentric contour lines. Here the cascade begins to form. In Fig. 9(b) the front of the cascade is just passing the computational box surface. Figure 9(c) shows the energy distribution long after the cascade front has left the plotted volume but yet before the cascade has started to interact with itself. Inclusion of the heat bath does not change the start of the cascade and the energy distributions are identical to those of Figs. 9(a) and 9(b). When reaching the surface region, the heat bath starts to affect the moving cascade front [Fig. 10(a)] and absorbs the cascade energy blocking its propagation. Figure 10(b), which is for about the same time as the end of the time period plotted in Fig. 8(b), reveals the possible energy reflection at the boundary to be minimal indeed. The last figure [10(c)] shows the energy distribution at the same time as Fig. 9(c), and, as can be seen, the distributions inside the computational box are of the same magnitude but the detailed forms are not quite alike. The largest kinetic energy encountered in these figures is about 17 r.u. This is much less than the lowest displacement threshold 118 r.u. found in Sec. III, and thus the atoms cannot cause any displacements in the cold parts of the solid. The path of the main cascade is seen to heat up to and beyond the melting point and cooling of this is somewhat different for the two cases, at least near the box boundaries.

The chosen width of the boundary region results in a reasonable energy outflow at the surfaces with little

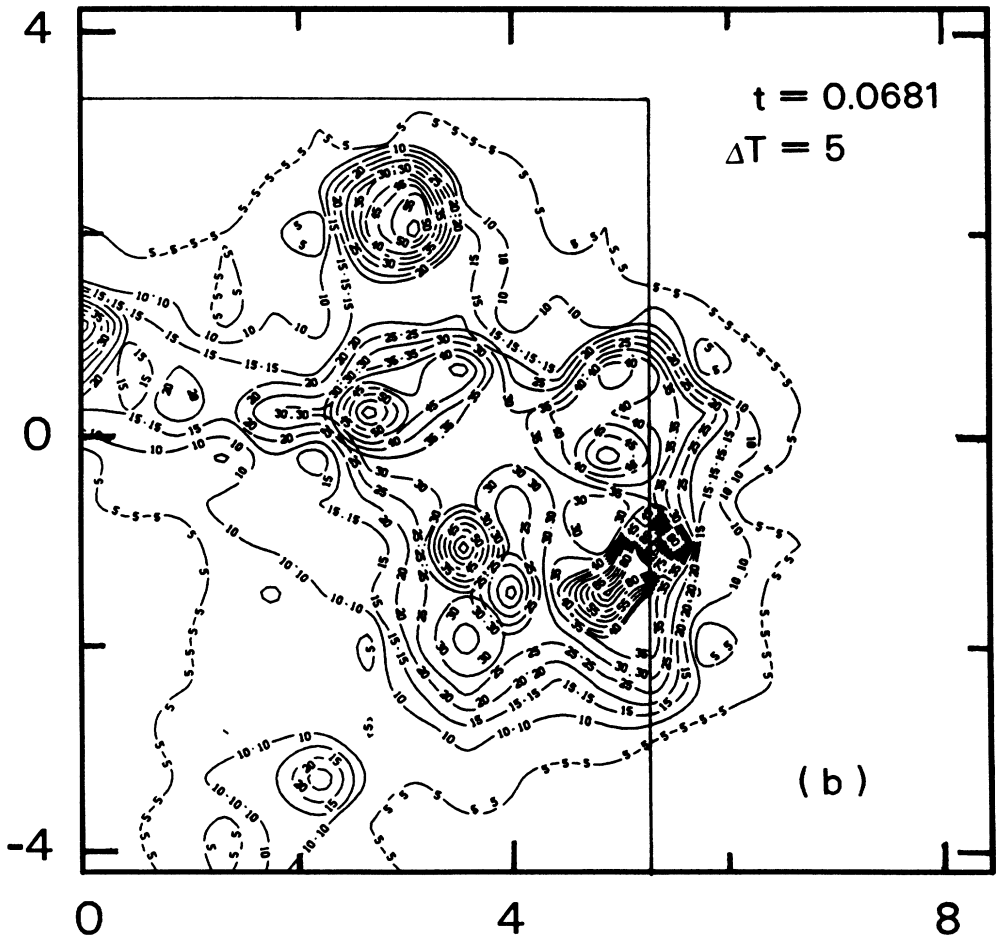

FIG. 9. (*Continued*).

reflection, while the advance of the cascade is effectively cutoff at the boundary. Possibly the most essential difference when compared with an infinite sample is in the initial stages of the radiation damage self-annealing, as especially near the boundary region the defect structure can be affected. The effect of the boundaries diminishes when going inside the computational box and also during the course of time, when the average temperature rapidly decreases. Doubling the width of the boundary region with less frequent scaling results in a slightly better energy dissipation and smaller distortion of the trajectories near the boundary. The small improvement is, however, outweighed by the larger number of the specially treated boundary region atoms.

V. RADIATION DAMAGE SIMULATIONS

We have studied the development of radiation damage in amorphous solids by performing collision-cascade simulations for ten different PKA energies ranging from 330 to 26 300 r.u. For each energy three different PKA positions and directions are used and thus a total of 30 collision cascades have been simulated. The PKA positions are within 2 r.u. from the computational box surface, and the energy impulse directions are chosen so that the computational box volume is utilized in the best way. In a real collision event the atoms will lose energy also in electronic interactions. A standard way to incorporate this effect into computer simulations is to subject the atoms to some energy loss per path length, which at low energies is proportional to the atomic velocity.[14] Electronic loss, however, is prominent for energies larger than those considered here, and the effect is not included in the present simulations.

Each simulation run consists of two parts: the first part is 1500 time steps long and simulates the initial stage of a cascade. During this the heat bath explained in Sec. IV is used. For the second part no heat bath is applied but instead at first (during 2000 time steps) the atomic velocities and the computational box volume are adjusted so that the sample temperature is about 0.028 r.u. with zero external pressure; finally a 1000-time-step-long equi-

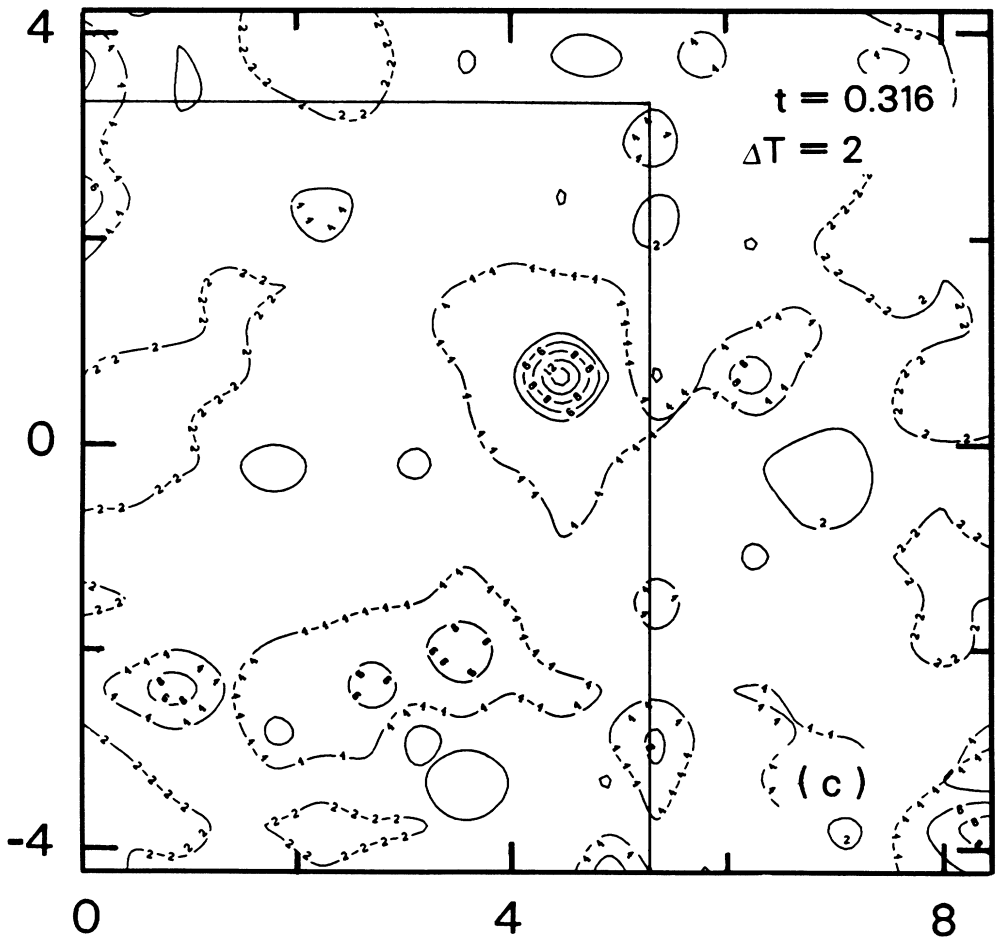

FIG. 9. (*Continued*).

librium period follows when no scalings are done. The first part simulates 10–16 r.u. of real time and the second one about 90 r.u. Initially the sample temperature is 0.0015 r.u. During the cascade it rises up to 12 r.u. for the highest PKA energies but because of the heat bath the temperature then decreases to 0.03 r.u. or less by the end of the first part.

Figure 11 shows a typical example of the initial stages of one collision cascade. It is clearly seen how the PKA energy is at first distributed to atoms situated in a cone, which has its tip at the PKA position and opens in the PKA direction. The cone formation is observed for all cascades; the cone angle is near 45° and appears to increase slightly with increasing PKA energy. In the figure one can also find a focusing sequence. Though focused sequences do not occur for every cascade, they are still very common, and one or more are seen for about half of the cascades. For a fixed PKA direction the focusing sequence usually stays the same for a large range of the PKA energies studied, but in one case we find the focusing sequence changes when the PKA energy is varied. The importance of the focused collisions lies in their ability to increase the extent of the radiation damage. In Fig. 11 one sees that a great number of atoms (that are not contained in the focusing sequence) experience large displacements, and thus they have considerable amounts of kinetic energy. The same applies to all focused collisions found. We correspondingly expect a focusing collision in an amorphous solid to receive less of the available energy than in a crystal. Also, because of the lack of periodic structure, the range of a focusing sequence is obviously shorter in amorphous materials. These reasons render focusing collisions to be of lesser importance in amorphous solids.

Figure 12 shows the number of vacancies and interstitials as a function of time for two PKA energies, 2000 and 11 500 r.u. The immediate observation is that the generation of point defects as a result of a collision cascade is a transient event and the defects vanish soon after they are created. The vacancies are seen to disappear in

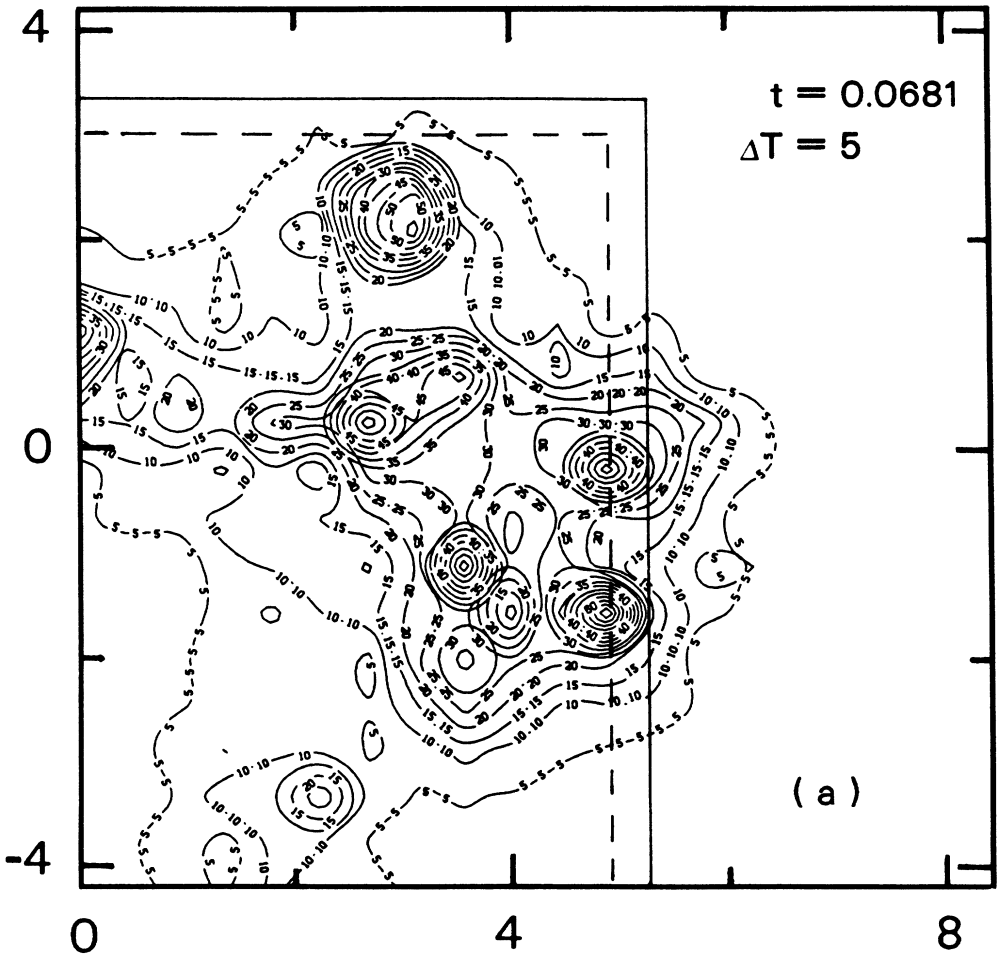

FIG. 10. The same as Fig. 9, but for the case of Fig. 8(b), where a heat bath is used.

1 and 3 time units for PKA energies of 2000 and 11 500 r.u., respectively. For interstitials these values are 7 and ~15 time units. Figure 12 is typical for all the cascades studied, with appropriate scaling by PKA energy. Specifically, at the end of a simulation run we find no vacancy left for any cascade and only one or two interstitials for nine of the 30 cascades. The existence of interstitials is not connected with the PKA energy and, in fact, reflects the typical equilibrium state of the sample (see II). Both defect types start to form at the same time but the interstitial maximum occurs slightly sooner than the vacancy maximum. The interstitials survive longer than the vacancies. The number of interstitials reaches maximum at about a time 0.19 r.u., and the vacancy number is at maximum around 0.29 r.u. Unexpectedly, these time instants turn out not to depend appreciably on the PKA energy; for vacancies, a very slight increase with increasing PKA energy is observed.

It has been explained in II that an interstitial can show up as increased local pressure for one to three atoms. Therefore in Fig. 12 we distinguish "all" and "distinct" interstitials: interstitials being nearest neighbors are counted as one in "distinct" values. It is seen that initially a large number of interstitial neighbors are created, but the local pressures are soon smoothed, and most of the surviving interstitials are distinct. The value of the PKA energy has an effect on the maximum interstitial number and the level at which the interstitial number sets after the first peak. The average maximum numbers of (distinct) interstitials and vacancies are plotted in Fig. 13 as a function of PKA energy. One sees that the number of interstitials grows very fast initially, but when the PKA energy increases the growth rate decreases, reaching saturation at around 15 000 energy units. The number of vacancies created is for low PKA energies smaller than that of interstitials. In this range the vacancy number increases linearly with PKA energy up to 11 500 r.u., after which the growth is somewhat slower but still faster than for interstitials. Beyond 16 500 r.u. more vacancies than interstitials are created. However, it is conceivable that

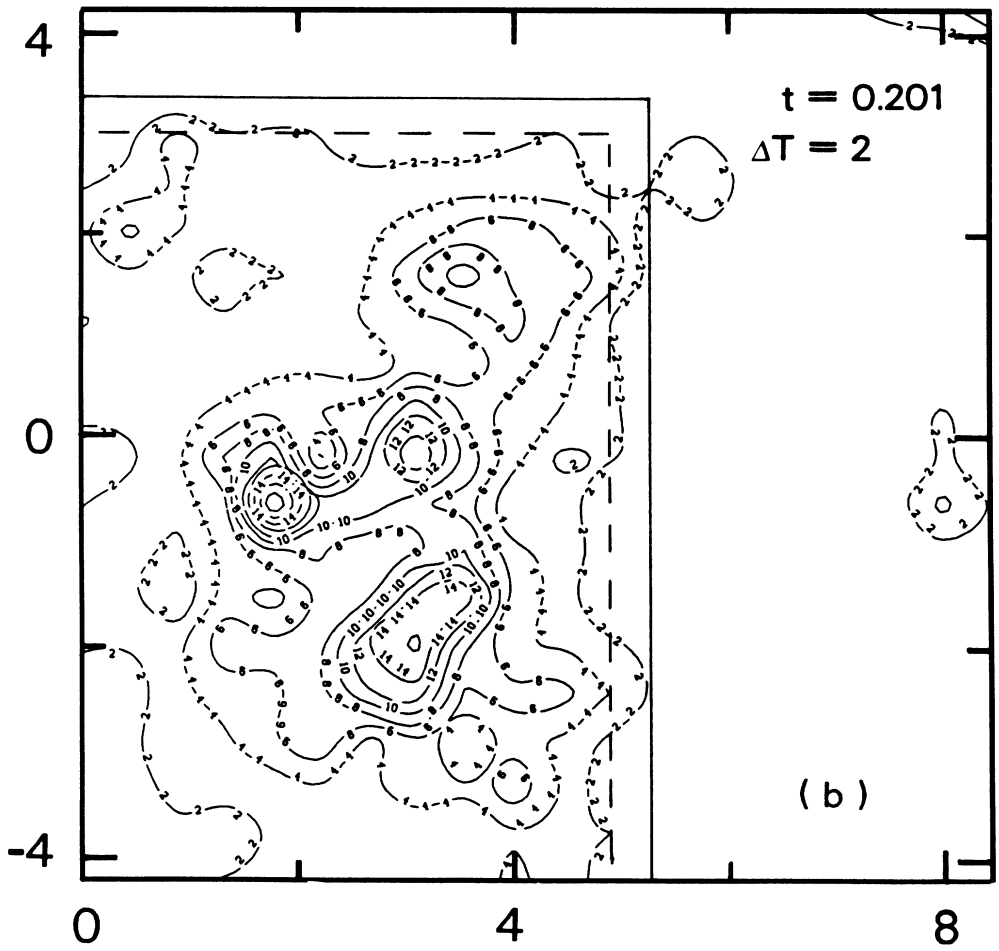

FIG. 10. (*Continued*).

the sample is too small for the largest PKA energies (> 15 000 r.u.).

Figure 14 shows the energy dependence of the (distinct) interstitial number right after the first peak is over and a slow decrease has set in. This happens at time $t \leq 0.42$ r.u. and can be determined rather accurately as seen, e.g., from Fig. 12(b). Now the interstitial value increases nearly linearly with the PKA energy up to 11 500 r.u. and, interestingly enough, this increase closely resembles that for the vacancies. After 11 500 r.u. the growth rate clearly changes. The slow decrease of the interstitial number after the first peak is approximately linear with time, as can be seen from Fig. 12(b).

Lindhard *et al.*[15] have given the following integral equation for the average number $\nu(E)$ of displacements produced by a PKA of energy E:

$$\int_0^E K(E,T)[\nu(T)+\nu(E-T)-\nu(E)]dT=0 , \quad (7)$$

where $K(E,T)$, the scattering law, is the probability that a particle with initial kinetic energy E will transfer kinetic energy T to another particle in a single collision. When analytically solving this equation it is usually assumed that (i) the cascade consists of binary elastic collisions, (ii) the displacement probability $P(E)$ is a step function $P(E)=\Theta(E-E_d)$, where E_d is the displacement threshold, and (iii) the energy E_d, consumed when making a displacement, can be neglected. Robinson[16–18] and Sigmund[19] have studied this equation in detail for various forms of the scattering law and the equation has been generalized to allow the particle also to move without making any collisions (describing channeling and replacement chains). In practice, however, the simple Kinchin-Pease model[1] has been widely applied instead. In addition to the preceding assumptions (i)–(iii) the Kinchin-Pease model considers only hard-sphere scattering and does not account for the crystal structure. With these assumptions one obtains, for the number of displacements,

$$\nu(E)=\begin{cases} 0 & \text{for } E<E_d \\ 1 & \text{for } E_d \leq E \leq 2E_d \\ \dfrac{E}{2E_d} & \text{for } 2E_d<E \ . \end{cases} \quad (8)$$

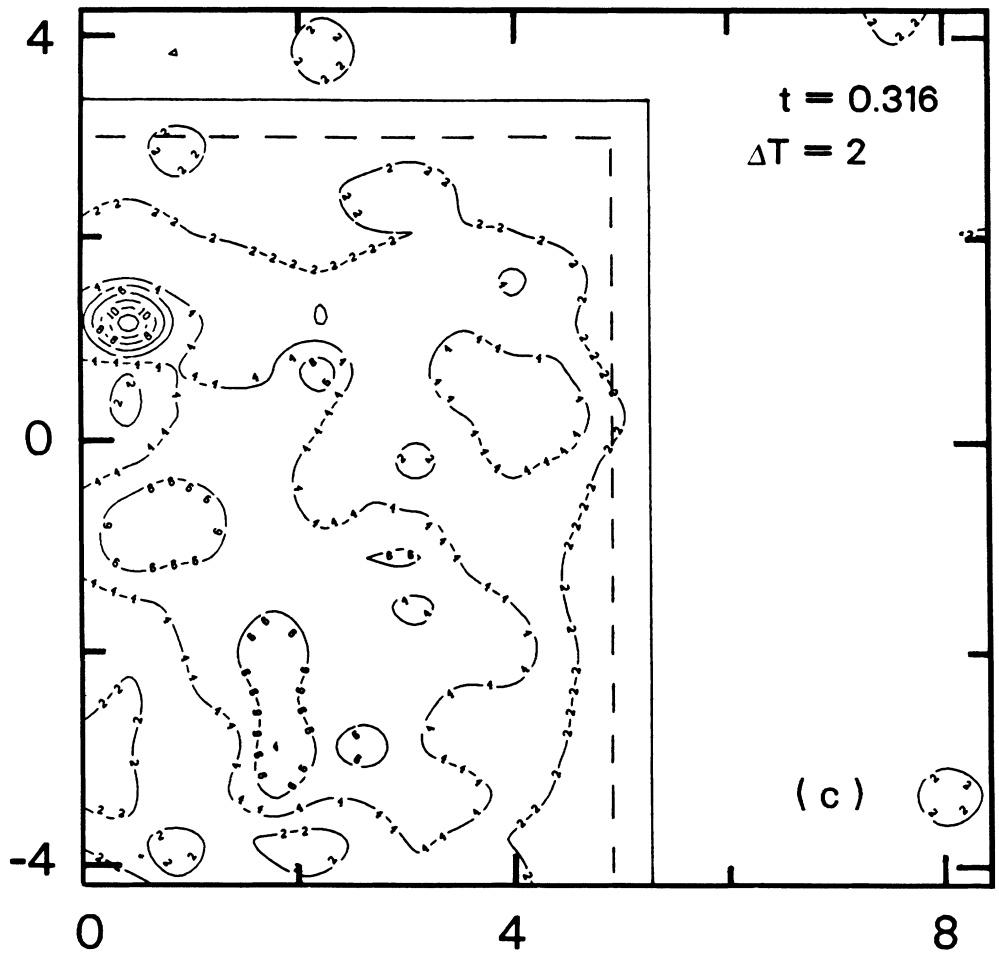

FIG. 10. (*Continued*).

The original Kinchin-Pease model has been later improved (the modified Kinchin-Pease model[15,19]) so that the number of displacements reads

$$\nu(E)=\begin{cases} 0 \text{ for } 0<\hat{E}<E_d \\ 1 \text{ for } E_d\le\hat{E}\le\frac{2}{\kappa}E_d \\ \frac{\kappa\hat{E}}{2E_d} \text{ for } \frac{2}{\kappa}E_d<\hat{E}\ . \end{cases} \tag{9}$$

Above, $\hat{E}$ is the energy actually left for damage production when the part spent for electronic excitations has been removed. The displacement efficiency κ is used to allow for deviation of the atomic interaction from a hard-core potential.

Excluding defect clustering, a displaced atom in a crystal along with the vacancy left behind forms a Frenkel pair and often one uses the number of Frenkel pairs as a synonym for the number of displacements. For amorphous solids, however, there is no more such correspondence. We thus consider explicitly the number of displacements when making a comparison with the Kinchin-Pease model. Since the displacement is defined here as a difference in the atomic position at two time steps instead of referring to a misalignment with respect to the periodic structure, it is important to properly choose the time instants, when the displacements are computed. The initial positions are, of course, those at the beginning of a simulation run. The end of the interval we set at a time when the kinetic energy of the fastest atom has been less than 118 r.u. at least for 30 time steps. This energy value is the lowest energy found in Sec. III to cause displacements, and thus the end of the interval marks the time when the cascade has ceased to expand and the number of defects created is about at maximum. For the minimum value of an acceptable displacement we

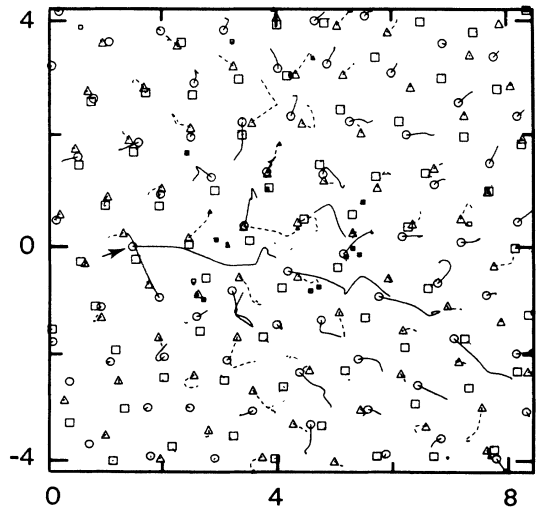

FIG. 11. Collision cascade caused by a PKA with the energy of 8200 r.u. The initial PKA position is shown by an arrow. The plot is made for the first 0.25 r.u. of time from the cascade start.

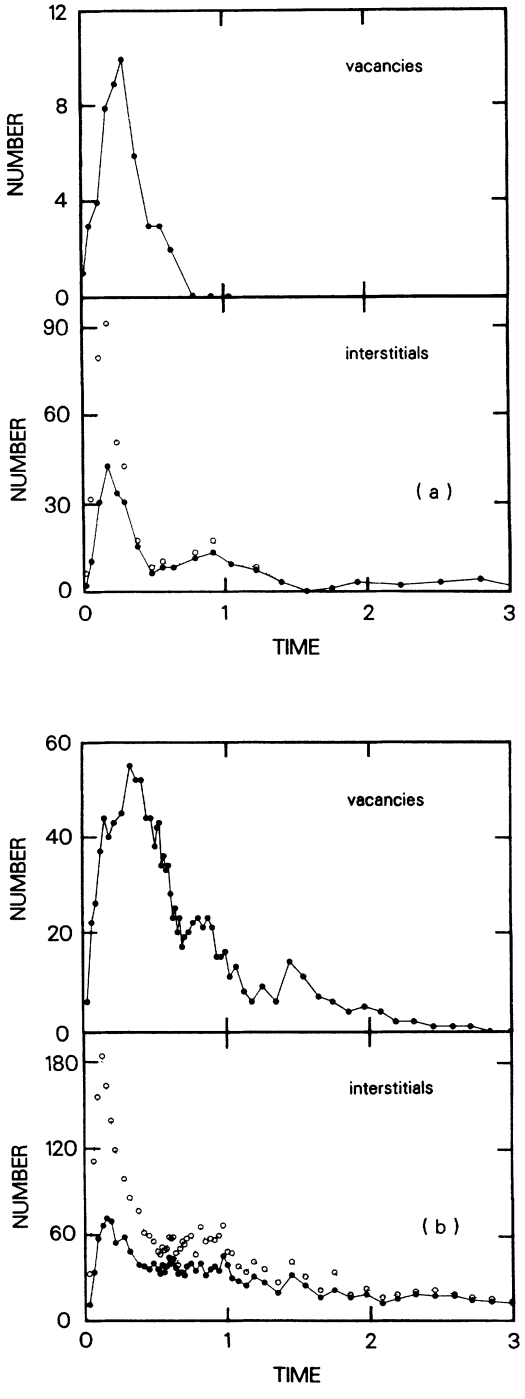

FIG. 12. The number of vacancies and interstitials as a function of time during a collision cascade. The PKA energy is 2000 r.u. in (a) and 11 500 r.u. in (b). For interstitials the open symbols show the number of all interstitial atoms and the solid symbols give the number of distinct interstitials (interstitials that are not nearest neighbors).

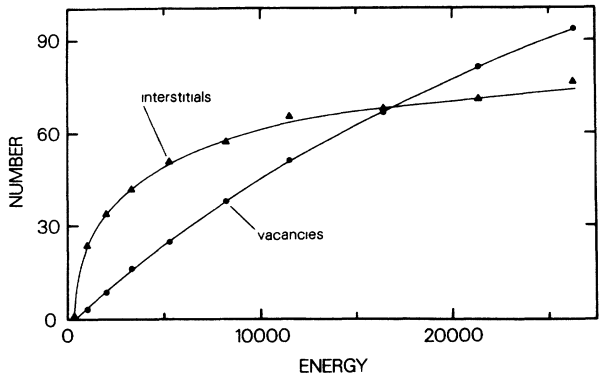

FIG. 13. The average maximum number of vacancies (circles) and distinct interstitials (triangles) as a function of the PKA energy. The values correspond to the maxima of curves like those in Fig. 12. The average of the three runs for each energy is given. The lines are drawn only to guide the eye.

use 1.07 r.u., i.e., the position of the first maximum of the pair distribution function. Figure 15 shows the number of displacements as a function of the PKA energy. The dependence is seen to be linear in energy up to 15 000 r.u.; thereafter the number of displacements appears to increase faster. A least-squares fit to a straight line for $E < 15\,000$ r.u. gives the energy prefactor 1.30×10^{-3} r.u.$^{-1}$. This is close to the Kinchin-Pease factor $\frac{1}{2}E_d = 1.14\times10^{-3}$ r.u.$^{-1}$, where for E_d the average value 440 r.u. from Sec. III is used. Using these results we obtain, for the displacement efficiency κ of the modified Kinchin-Pease model, an energy-independent value at 1.14. As a comparison, for crystals the constant value $\kappa = 0.8$ has been generally accepted.[20,21] At large energies more defects are produced than the linear increase would indicate. But, in accordance with the preceding discussion, this is obviously an artifact due to the small sample:

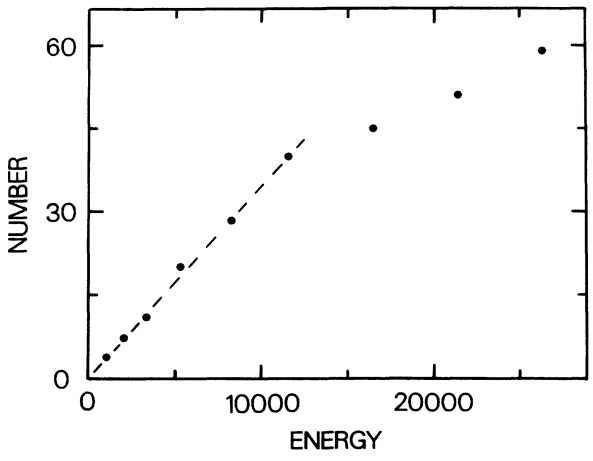

FIG. 14. The number of distinct interstitials at the time when the maximum defect number has been passed and the rapid decrease is changing to a more slowly vanishing rate of interstitials.

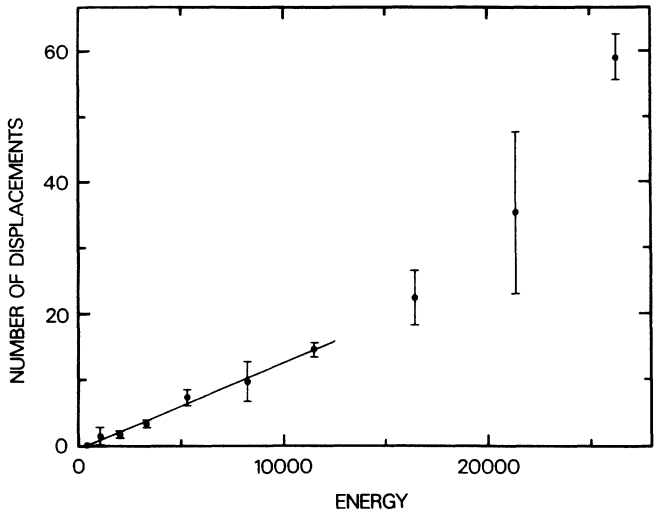

FIG. 15. Number of displacements as a function of energy of the PKA atom. The circles show the average and the bars indicate the standard deviation of the three separate collision-cascade simulations done for each energy. The line is a least-squares fit for energies below 15 000 r.u.

the boundary conditions apparently do not allow for the largest PKA energies to spread out fast enough but constrain the energy in a relatively small volume for too long a time and thereby increase the displacement number. Note that the criterion used here for the end of the displacement time interval corresponds to the moment, when all the possible displacements caused by the PKA have been made. This choice is consistent with the Kinchin-Pease model, where an atom after being displaced is not assumed to recombine with a vacancy. King and Benedek find, too, that the number of Frenkel pairs in their crystal simulation corresponds to the Kinchin-Pease value when the Frenkel pairs are counted in the end of the collisional or defect generation phase (when the number is at maximum).[13]

The Kinchin-Pease model sets a sharp cutoff for $\nu(E)$

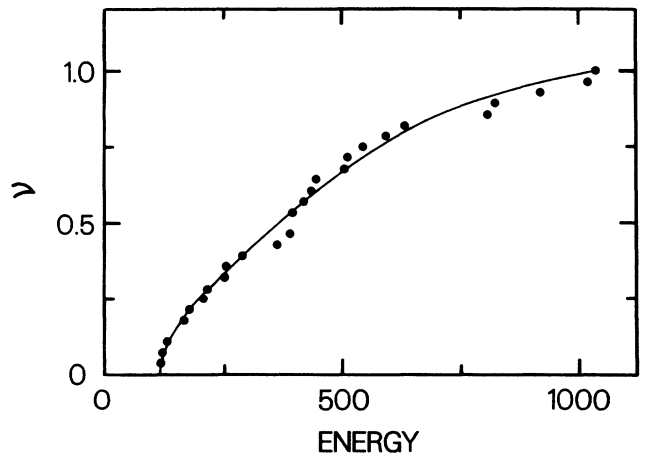

FIG. 16. Number of displacements at low PKA energies as determined by Eq. (10).

at the displacement energy E_d. However, as is evident from Fig. 6, the displacement threshold actually depends on the direction: $E_d = E_d(\Omega)$. Correspondingly, King *et al.*[22] define $\nu(E)$ for energies near E_d by

$$\nu(E) = \int_\Omega \Theta[E - E_d(\Omega)] \frac{d\Omega}{4\pi} . \quad (10)$$

In Fig. 6 values of $E_d(\Omega)$ for one atom have been presented. Using this data Fig. 16 shows $\nu(E)$ for $\nu \leq 1$ as determined according to Eq. (10). For a crystal, the qualitative features of $\nu(E)$ are a sharp increase at the minimum threshold energy and an extended plateau at a value $\nu(E) < 1$.[13,23] Both of these are assumed to be a result of the periodic structure. Figure 16 indicates that in the case of an amorphous solid $\nu(E)$ does not rise abruptly from zero, nor is there a distinct plateau before $\nu(E)$ attains the value 1.

The actual positions of vacancies and interstitials for a typical cascade are depicted in Fig. 17. This is the same collision event as considered in Fig. 12(b). The PKA energy is 11 500 r.u., and Fig. 17(a) shows the atomic movements during the first 0.44 time units. At the very beginning of the cascade vacancies appear near the initial position of the PKA, while interstitials are created further away by the advancing cascade front. Right after this [Fig. 17(b), time is 0.095 r.u.] vacancies are also formed

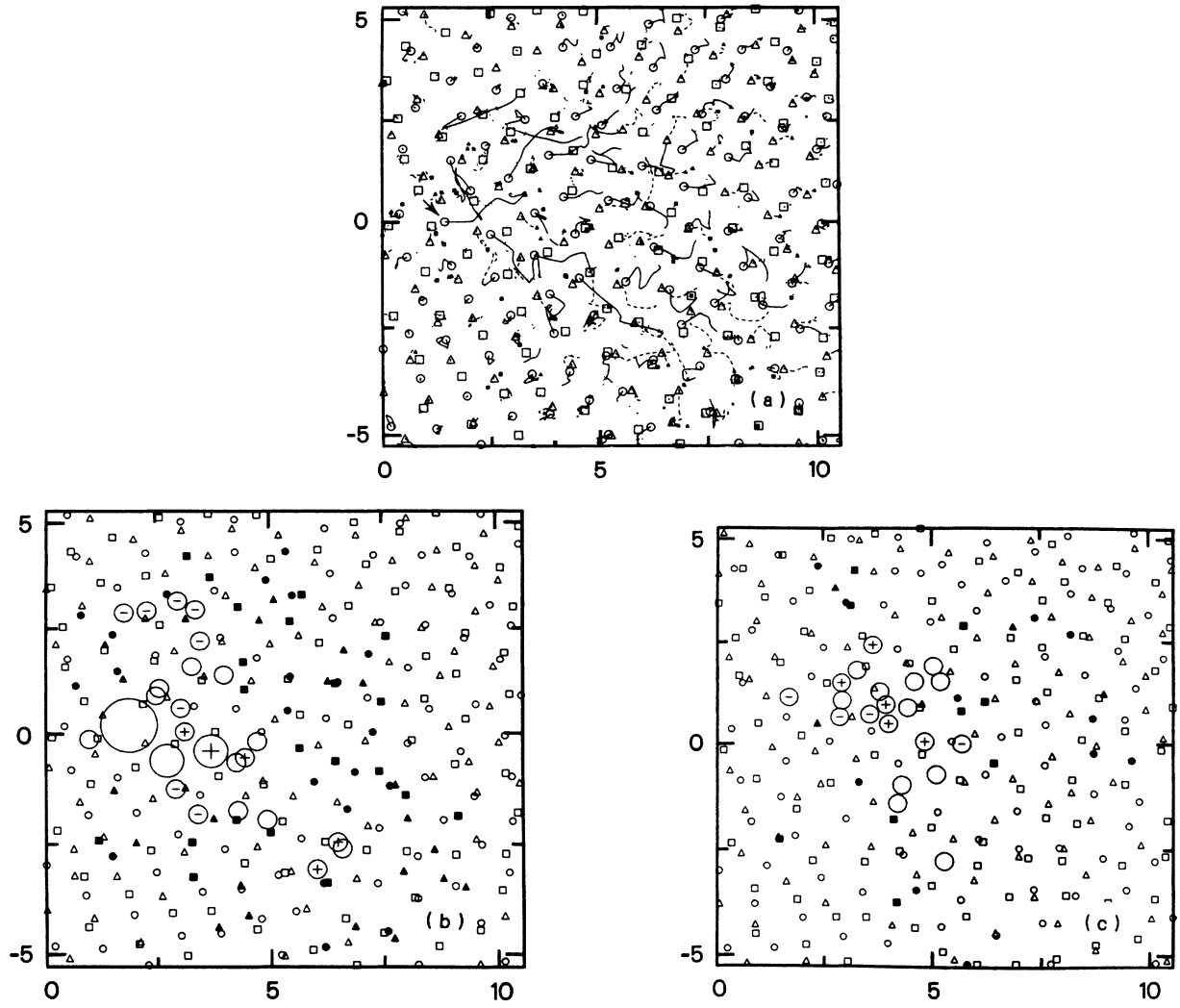

FIG. 17. A collision cascade initiated by a PKA atom with an energy 11 500 r.u. (a) shows atomic trajectories within 0.44 time units from the beginning of the cascade. The initial PKA position is indicated by an arrow. (b) and (c) show the locations of defects and atoms at times 0.095 and 0.67 r.u., respectively. Noninterstitial atoms are plotted as described earlier. The interstitial atoms are indicated as solid symbols. Cavities of various sizes are represented by circles of different diameters d depending on the cavity volume V: if $V < 0.49$ r.u., then $d = 3d_0$ (d_0 is the diameter of the sphere representing an atom), for $0.49 \leq V \leq 0.98$ r.u., $d = 5.4d_0$ (this is the volume range for clusters of two or three vacancies) and for $V > 0.98$ r.u., $d = 9d_0$. A + or − sign inside a cavity sphere indicates that the cavity is in the upper or lower third of the plotted volume. All the plotted volumes in (a)–(c) are oriented in the same way.

along the cascade, making some of the initially created interstitials vanish. The majority of the interstitials are found at the outer parts of the cascade. At the time when the numbers of vacancies and interstitials have passed their maxima [Fig. 17(c), time is 0.67 r.u.; see also Fig. 12(b)] the vacancies are seen to be located close to each other near the beginning of the cascade, and the interstitials are further away surrounding the vacancies. In spite of the vacancies being close to each other, we typically do not find them to form large clusters. The vacancy distribution also keeps changing somewhat, while the defect numbers decrease continuously. Later, at time 2 r.u., only a few defects exist; the vacancies are still approximately in the central region of the cascade volume and the interstitials in the outer parts. No distinct defect complexes are found.

The correlations between the defects can be studied quantitatively by computing the pair distribution functions for cavity-cavity [denoted as $g_{cc}(r)$], interstitial-interstitial [$g_{ii}(r)$], and cavity-interstitial [$g_{ci}(r)$] pairs. We have done this for the cascade considered earlier in Figs. 12(b) and 17. Figure 18(a) shows the pair distribution functions in the beginning of the simulation at time 0.066 r.u., when the cascade is rapidly growing and the defect numbers have not reached their maxima [cf. Fig. 12(b)]. At the time of Fig. 18(b) (time 1.26 r.u.) the so-called short-term annealing has started and most of the defects created have already vanished. The cavity-cavity correlation does not change considerably during the course of time: a prominent peak is seen at 0.75 r.u. with a rapidly decreasing tail. The peak is due to several proximate cavities forming a vacancy and the short tail indicates that the cavities (vacancies) created are situated within a limited region. The interstitial-interstitial distribution, too, has a clear peak at short distances but the tail is clearly longer than for cavities and becomes more uniform with time. The long tail manifests quantitatively the fact evident in Fig. 17, i.e., that the interstitials are rather evenly distributed in a large volume. Previously in II it has been stated that the interstitials appear often as nearest-neighbor pairs. This can also be seen from the interstitial-interstitial distribution function in Fig. 18 as the sharp peak at 0.9 r.u. The cavity-interstitial correlation function follows the spreading of the interstitials along with the cascade front. An interesting feature is the prominent peak at 0.94 r.u. indicating of the existence of some close cavity-interstitial pairs. Moreover, unlike g_{cc} and g_{ii}, the cavity-interstitial distribution func-

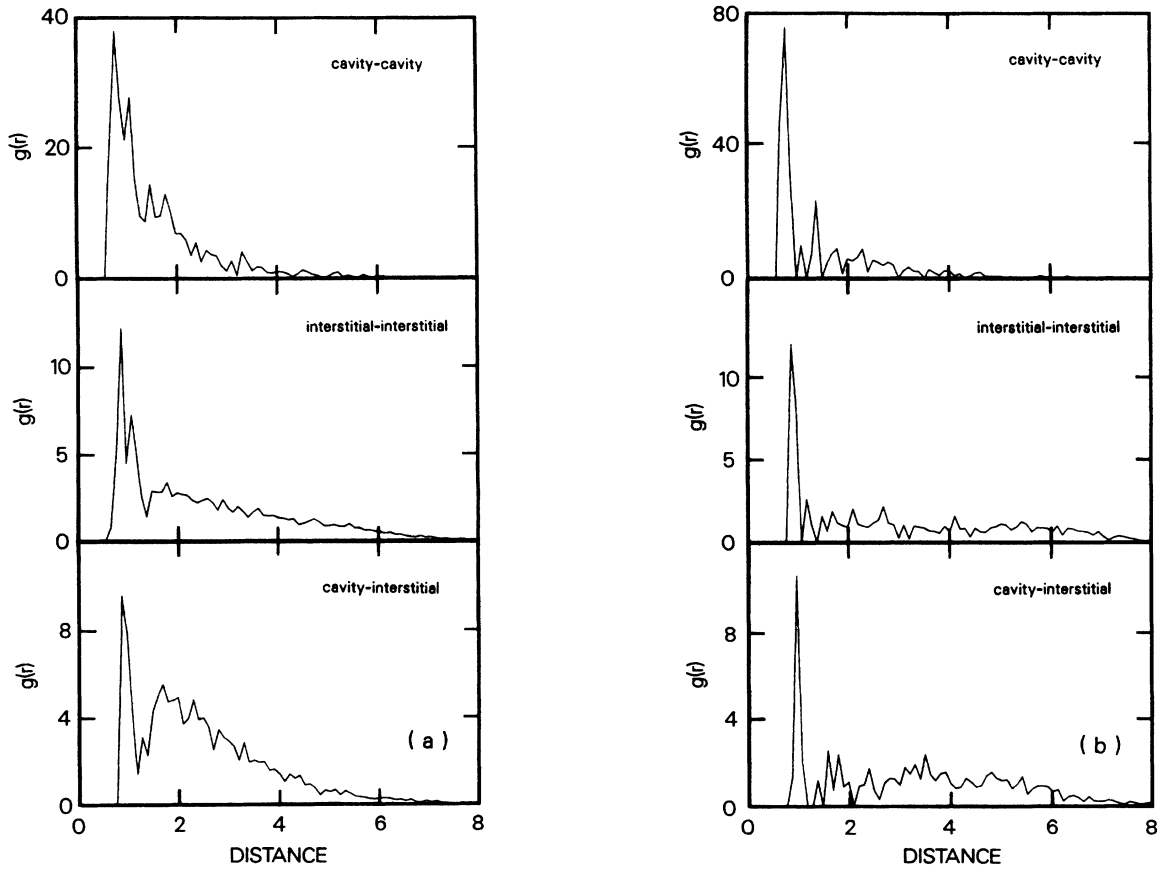

FIG. 18. The different defect pair distribution functions of the collision cascade in Fig. 17 at (a) $t=0.066$ r.u. and (b) $t=1.26$ r.u.

tion is seen to vary to some extent during the annealing, and one case has been found where the peak at 0.94 r.u. is disappeared.

From the pair distribution functions one can easily compute the average distances between various defect pairs. This is done for the cascade considered earlier and the average distances are plotted in Fig. 19 as a function of time. After the rapid initial increase (following the cascade expansion) at time $t \simeq 0.4$ r.u. the average cavity-cavity distance is 3.8 r.u., whereas the interstitial-interstitial and cavity-interstitial distances (~ 5.2 r.u. for both) are considerably larger. Apart from fluctuations, the average distances are seen to decrease slightly with time, and no abrupt changes take place.

A point defect in an amorphous structure can vanish, in principle, by two different mechanisms: a vacancy and an interstitial may annihilate each other through recombination or the immediate neighborhood of a defect can slightly rearrange itself and thereby dissolve the extra volume of a vacancy or ease the pressure of an interstitial atom (we call this mechanism the collective mode). For crystals the recombination (excluding the diffusion to the surface and trapping at grain boundaries, etc.) is the only possibility. Considering the relative importance of the two mechanisms in short-term annealing of collision cascades some conclusions can be drawn from the pair distribution functions. If the recombination were the principal annealing mechanism then one might expect the first peak of the cavity-interstitial distribution function to diminish as the defects annihilate, and the average cavity-interstitial distance should increase. In order to quantitatively study the number of close cavity-interstitial pairs we consider the integral

$$N_{\mathrm{ic}} = \frac{4\pi \int_0^R g_{\mathrm{ci}}(r)\,dr}{N_c}, \tag{11}$$

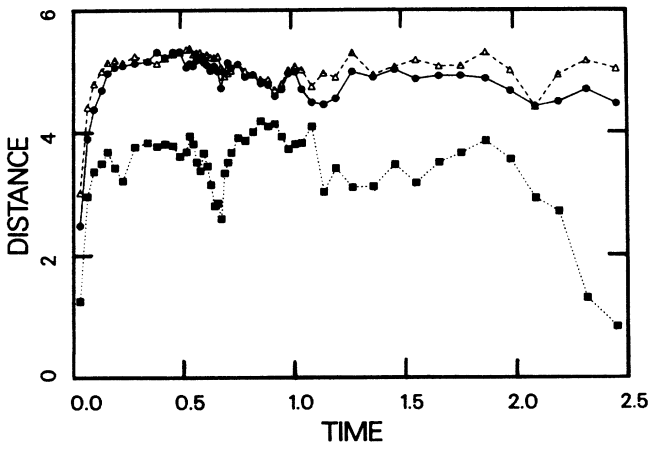

FIG. 19. Average distances between the defect pairs as a function of time. Squares show cavity-cavity distance, triangles are for interstitial-interstitial pairs, and circles denote cavity-interstitial distance. The data are from the collision simulation of Fig. 17.

where N_c is the number of cavities and $R = 1.24$ r.u. so that the integration region just includes the first peak of g_{ci}. N_{ic} is thus proportional to the number of interstitials per one cavity that are closer than 1.24 r.u., and we use it to estimate the prerequisites for recombination. At the first time instant studied ($t = 0.032$ r.u.) $N_{\mathrm{ic}} \simeq 1$, but when the cascade expands N_{ic} drops to $0.1, \ldots, 0.2$ within 0.2 time units and subsequently does not change considerably. Obviously a recombination event would show up as a simultaneous decrease in N_{ic} and the number of cavities and interstitials. A few such events are found, but they cannot account for the most of the defects vanished. As a result we conclude the collective mode to be the main annealing mechanism. This is also supported by the observation that $g_{\mathrm{ii}}(r)$ changes only very slightly in time, indicating a stable interstitial distribution. Yet a significant recombination rate would require a fast interstitial diffusion, we have found that the cavities do not move appreciably before dissolving.

Computer simulation makes it possible to study whether changes in volume and structure because of only one PKA occur. Since small changes are considered, it is important that the equilibrating procedure described previously is adequate. To study this we have simply performed another 3000-time-step-long equilibrium run after the first one for some of the cascades. All of the results show no changes in the volume of the sample or in the structure as disclosed by the pair distribution function, and thus the cascades can be considered as having reached quasiequilibrium in the end of a simulation run. The change ΔV in the sample volume is seen to lie in the range -0.46–0.12 % of the initial volume, and its average is negative. However, the sign and magnitude of ΔV varies randomly with increasing PKA energy. Thus the observed changes in ΔV are to be considered only as statistical variation, and no definite conclusions of the volume change can be drawn. Changes in the structure are studied by comparing the pair distribution function before and after a collision cascade. The changes turn out to be very small; mainly the position and the height of the first peak may vary in minute amounts, and, as before, the changes are of a statistical rather than a systematic nature.

VI. DISCUSSION

A common question concerning the quantitative reliability of MD simulation results is what the role of the potential used is. Besides the detailed form of the potential, the applicability of the pair potential formulation in general has also been discussed. Also the density dependence of the potential has been scrutinized. Metals can be divided into two broad classes: simple and nonsimple metals. The former are nearly-free-electron metals with tightly bound electron cores, which do not overlap appreciably with the cores of neighboring atoms. For these the pair potential concept finds justification via pseudopotential perturbation theory. The situation is different for the nonsimple metals, a typical example of which are the transition metals. Because of the d-band effects it is questionable whether the energy of a transition metal can be

expressed as a sum of pair potentials and recipes for many-atom interactions have been proposed.[24–26] MD practitioners, however, have used semiempirical pair potentials for transition metals with considerable success for selected problems. The Lennard-Jones potential used here is physically suitable for solid noble gases, but the results obtained can help elucidate the generic properties of disordered systems.

Formation of radiation damage is accompanied with changes in the local density of the solid, and correspondingly one is faced with the possible density dependence of the potential and its effect on the defect structure.[27] According to Taylor[28] the density dependence of a potential affects the energy changes associated with a defect more than its structure. This applies even for extended defects such as grain boundaries (but not free surfaces) and Taylor concludes that a density-independent potential can be used to give a reasonable defect structure.

The question of density dependence also touches upon the constraints of the simulation. de Leeuw *et al.*[29] have directly compared the results obtained using constant-pressure and constant-volume simulations. They find the ensembles yield the same static and short-term dynamical properties but observe slight differences at large times (e.g., different diffusive behavior). In the present work these findings are accounted for by adjusting the sample volume (i.e, using in effect a constant-pressure simulation) for the second part of the cascade when the short-term annealing is taking place. For the initial collisional and final equilibrium states the constant-volume simulation is applied.

In this work a new method of accomplishing the energy dissipation at boundaries has been introduced. The method uses a boundary region and energy scaling, which are easy to include in the simulation algorithm, and the appropriate parameter values can be readily determined applying the criteria given. We consider the parameter set used here a fair compromise between the various requirements, and the physically important requirements for the boundary conditions, reasonable energy outflow from the sample and little affect on the cascade structure, were seen to be attained. Obviously, there is always room for discussion of the optimal parameter choice or the best way to include the energy outflow in the simulations, but, on the other hand, there are indications that the simulation results, after all, are not very sensitive to the boundary effects.[5] Another question is the size of the computational box (the number of atoms). The results of the simulations indicate that the present sample size may be too small for large PKA energies ($E > 15\,000$ r.u.) and correspondingly one should keep this possibility in mind when examining the outcome of high-energy cascades.

Figure 6 shows the displacement threshold energy to depend sharply on the displacement direction. This is slightly surprising, since a disordered structure might lead one to expect more smooth variations. On the other hand, King and Benedek find a rather similar rapidly varying threshold energy curve for crystalline Cu in their simulations,[13] and Audouard *et al.* experimentally reach the conclusion that amorphous and crystalline $Fe_{75}B_{25}$ have the same displacement threshold energy.[30] King and Benedek also discover similar easy and hard directions and a stepwise type of displacement as found in this work. Likewise the atomic trajectories for both structures exhibit replacement collision sequences with effective energy transfer from atom to atom. It seems, in fact, that the displacement threshold energy has many features common for both the crystalline and amorphous structures. This indicates that the displacement threshold is determined by the immediate vicinity of an atom and does not probe the long-range order of the material. The ratio of E_d minimum (118 r.u., 0.36 eV for Ne) to the cohesive energy of a solid noble gas [0.02 eV for crystalline Ne (Ref. 31)] is about two times as much as that for crystalline Cu [$E_{d,\min} \simeq 25$ eV,[5,13] cohesive energy is approximately 3.5 eV (Ref. 32)]. Allowing for the definition of a displacement and the exact value of cohesive energy for the amorphous structure, these numbers suggest that the displacement threshold is slightly larger for the disordered than for the crystalline structure.

The collision cascades were seen to exhibit features such as replacement and focused collision sequences. In this case a focused chain means collisions propagating via a string of densely packed neighboring atoms rather than atoms scattering into definite angles. In addition, now the focused chain has a curved trajectory and gives off energy more rapidly than in a crystal. In general, the cascade was observed to expand initially into a cone-shaped form, which results in a fast spreading of cascade energy thereby reducing the extent of the affected region. Replacement collisions and rapid branching of the cascade have also been seen in simulations of amorphous iron by Yamamoto *et al.*[33]

A study of the temporal properties of the point defect numbers revealed that the interstitial number is at its maximum slightly before that for vacancies, and these time instants change only little with the PKA energy. The minor energy dependence of the time corresponding the maximum number can also be seen in cascade simulations for a crystalline structure.[21] The time instant at a maximum number appears to be a fraction of a pico second, the exact value depending on the potential strength and the atomic mass.

The PKA energy directly affects the maximum numbers of defects. The vacancy number increases nearly linearly with the PKA energy, for high energies slower than for small energies. The prompt interstitial number initially rises very fast but levels off at large energies. The vanishing of defects is slower for interstitials than for vacancies. Finally, after equilibrating, no vacancies and only 0–2 interstitials were observed. The interstitials were further connected with the normal, semiequilibrium state of the sample rather than resulting from the collision cascade. These findings are clearly in contrast with simulations for crystalline samples, where stable Frenkel pairs or displacements after cascades are routinely seen. Comparing the present results with those obtained for a similar sample by Chaki and Li,[34] the time of reaching the maximum interstitial number is the same for both, but otherwise the time development of the defect numbers are different; for example, Chaki and Li find that the vacancies disappear more slowly than the interstitials.

The reason for this probably lies in the different description of point defects and the simulation algorithm itself. (Chaki and Li use Voronoi volumes for defect identification, and they do not allow for energy outflow at the boundaries.) At the end of a collision simulation Chaki and Li do not find any new defects, either.

A study of the defect positions revealed that the vacancies are created near the PKA position at the center of the cascade and the interstitials spread around them. This is an interesting observation, as the same is known also to happen with crystals.[5,13,22] In spite of being close to each other no vacancy clustering was seen; on the other hand, the vacancies exist only a short time before vanishing. The defect pair correlation functions showed the interstitials to be distributed rather evenly around the vacancies. The computed average vacancy-vacancy distance appears to be considerably less than the vacancy-interstitial or interstitial-interstitial distances supporting the suggested picture. The pair distribution functions also helped to differentiate between the two main possibilities of short-term annealing: a mutual recombination of a vacancy and an interstitial or individual vanishing of a defect. We suggest the latter; recombination would presume a significant mobility of the interstitials, which is improbable because of the stable interstitial distribution. Low mobility of interstitials is also supposed by Chaki and Li. On the other hand, individual vanishing of defects is clearly needed to make the vacancies and interstitial disappear at different rates.

In order to compare the results with the predictions of the modified Kinchin-Pease model, we determined the number of displacements at the moment, when the cascade has ceased to expand and the defect number is around its maximum. Because of the missing periodicity, a displacement is defined here directly as a difference of an atom's position at two time instants. Following the Kinchin-Pease model the displacement number turned out to increase linearly with PKA energy, except for large energies where the increase is more rapid. With the displacement threshold $E_d = 440$ r.u. we obtained, for the displacement efficiency, $\kappa = 1.14$, which should be compared with the value 0.8 often used for metals. We find this correspondence to further support the value proposed here for E_d. Obviously, an exact value of E_d cannot be set unequivocally, and, e.g., for Cu the value $E_d = 25$ eV is used often even if Gibson *et al.* find the displacement threshold to vary between 25 and 85 eV.[5] Note that a smaller value of E_d would correspondingly decrease κ, too. The curve for the number of displacements near the threshold ($\nu \leq 1$) turned out not to clearly exhibit the features typical for crystals: a sharp increase and a distinct plateau. This we consider to follow from the lack of periodicity in an amorphous structure so that the existing short-range order is not enough to produce these details. Further studies would be in order to collect more statistics for other directions.

It is well known that heavy irradiation causes swelling especially in crystalline but to some extent also in amorphous metals.[35] Computer simulation with periodic boundary conditions is capable of disclosing changes in the sample volume as observed, e.g., in publication I when preparing the amorphous structure from a crystal. We checked this for swelling due to a collision event but found no systematic changes in the sample volume or the pair distribution function. This is not surprising, since only one PKA in the sample corresponds to a very minute dose, and many more cascades (one following the other) would be needed to simulate the doses observed to cause swelling. However, Yamamoto *et al.* report distinct changes in the pair distribution function after only one cascade.[33]

VII. CONCLUSIONS

A computer simulation study of radiation damage in an amorphous solid involves a proper simulation technique and a practical way to identify point defects in the structure. The latter subject has been studied in our earlier publication (II). In this work the usual MD method has been modified to allow for energy outflow through the computational box surfaces and constant-pressure simulation has been applied during defect annealing. The 30 collision-cascade simulations made show the energy of a PKA to be rapidly distributed to nearby atoms, and as a result the affected cascade volume is limited. Collision sequences such as replacement collisions and focused chains are observed. The defect structure is found to be composed of mostly vacancies in the center with evenly distributed interstitials around. All the defects turn out to be unstable: the vacancies disappear in 1–3 time units; interstitials have a longer lifetime. We conclude that the defects vanish independently of each other. The easiness of point defect annealing and the limited cascade volume are obvious reasons for the abnormally good radiation resistance of amorphous solids. The number of defects created increases with the PKA energy, but the time instant when the defect number is at maximum is not appreciably affected by it. The displacement threshold energy as a function of ejection angle is determined and is found to show considerable variation. The number of displacements computed from the cascades is seen to increase linearly with the PKA energy and with an average displacement threshold energy reasonable compatibility with the modified Kinchin-Pease model is obtained. The sample volume and pair distribution function show no systematic changes before and after a collision cascade.

In this work a one-component system with the simple Lennard-Jones pair potential has been studied and no electronic losses are included. These are obviously not the conditions prevailing in a real amorphous metal. However, in addition to increasing the knowledge of the properties of amorphous Lennard-Jones systems we expect these studies to reveal many of the general properties of amorphous solids.

ACKNOWLEDGMENTS

We are grateful to Dr. M. Manninen for useful discussions and Mr. T. Siili for his extensive participation in creating the computer programs for graphical presentation of collision-cascade data.

*Present address: Okmetic Ltd., P.O. Box 44, SF-02631 Espoo, Finland.
[1]G. H. Kinchin and R. S. Pease, Rep. Prog. Phys. **18**, 1 (1955).
[2]J. R. Beeler, *Radiation Effects Computer Experiments* (North-Holland, Amsterdam, 1983).
[3]H. L. Heinisch, J. Nucl. Mater. **117**, 46 (1983).
[4]T. Muroga and S. Ishino, J. Nucl. Mater. **117**, 36 (1983).
[5]J. B. Gibson, A. N. Goland, M. Milgram, and G. H. Vineyard, Phys. Rev. **120**, 1229 (1960); see also C. Erginsoy, G. H. Vineyard, and A. Englert, *ibid.* **133**, A595 (1964).
[6]J. Yli-Kauppila, Ph.D. thesis, Helsinki University of Technology, 1983.
[7]A. Audouard, J. Balogh, J. Dural, and J. C. Jousset, J. Non-Cryst. Solids **50**, 71 (1982).
[8]S. Cui, R. E. Johnson, and P. Cummings, Surface Sci. **207**, 186 (1988).
[9]J. Laakkonen and R. M. Nieminen, J. Non-Cryst. Solids **75**, 237 (1985).
[10]J. Laakkonen and R. M. Nieminen, J. Phys. C **21**, 3663 (1988).
[11]D. O. Welch, G. J. Dienes, and A. Paskin, J. Phys. Chem. Solids **39**, 589 (1978).
[12]D. Beeman, J. Comput. Phys. **20**, 130 (1976).
[13]W. E. King and R. Benedek, J. Nucl. Mater. **117**, 26 (1983).
[14]J. Lindhard, M. Scharff, and H. E. Schiøtt, Mat. Fys. Medd. Dan. Vid. Selsk. **33**, No. 14 (1964).
[15]J. Lindhard, V. Nielsen, M. Scharff, and P. V. Thomsen, Mat. Fys. Medd. Dan. Vid. Selsk. **33**, No. 10 (1963).
[16]M. T. Robinson, Philos. Mag. **12**, 741 (1965).
[17]M. T. Robinson, Philos. Mag. **17**, 639 (1968).
[18]M. T. Robinson and O. S. Oen, J. Nucl. Mater. **110**, 147 (1982).
[19]P. Sigmund, Radiat. Eff. **1**, 15 (1969).
[20]M. J. Norgett, M. T. Robinson, and I. M. Torrens, Nucl. Eng. Des. **33**, 50 (1975).
[21]M. W. Guinan and J. H. Kinney, J. Nucl. Mater. **103&104**, 1319 (1981).
[22]W. E. King, K. L. Merkle, and M. Meshii, Phys. Rev. B **23**, 6319 (1981).
[23]K. L. Merkle, W. E. King, A. C. Baily, K. Haga, and M. Meshii, J. Nucl. Mater. **117**, 4 (1983).
[24]F. Ercolessi, E. Tosatti, and M. Parrinello, Phys. Rev. Lett. **57**, 719 (1986).
[25]S. M. Foiles, M. I. Baskes, and M. S. Daw, Phys. Rev. B **33**, 7983 (1986).
[26]K. W. Jacobsen, J. K. Nørskov, and M. J. Puska, Phys. Rev. B **35**, 7423 (1987).
[27]R. N. Barnett, C. L. Cleveland, and U. Landman, Phys. Rev. Lett. **55**, 2035 (1985).
[28]R. Taylor, J. Phys. (Paris) Colloq. **46**, C4-309 (1985).
[29]S. W. de Leeuw, M. Dixon, and R. J. Elliott, Philos. Mag. A **46**, 677 (1982).
[30]A. Audouard, J. Balogh, J. Dural, and J. C. Jousset, Radiat. Eff. **62**, 161 (1982).
[31]N. W. Ashcroft and N. D. Mermin, *Solid State Physics* (Holt, Rinehart and Winston, New York, 1976).
[32]W. A. Harrison, *Electronic Structure and the Properties of Solids* (Freeman, San Francisco, 1980).
[33]R. Yamamoto, H. Shibuta, and M. Doyama, J. Nucl. Mater. **85&86**, 603 (1979).
[34]T. K. Chaki and J. C. M. Li, Philos. Mag. B **51**, 557 (1985).
[35]B. T.-A. Chang and J. C. M. Li, Scripta Metall. **11**, 933 (1977).